Structure of FeI_2·[16]aneS_4: Square-Planar or Octahedral Iron Coordination?

H. Paulsen,[†] M. Kröckel,[†] M. Grodzicki,[†] E. Bill,[†] A. X. Trautwein,*[,†] G. J. Leigh,[‡] and J. Silver[§]

Institut für Physik, Medizinische Universität zu Lübeck, D-23538 Lübeck, Germany, School of Chemistry and Molecular Sciences, University of Sussex, Brighton BN1 9QJ, U.K., and Department of Chemistry and Biological Chemistry, University of Essex, Colchester CO4 3SQ, U.K.

Received May 3, 1995[⊗]

The adducts FeI_2·[16]aneS_4 (**1**) and $FeBr_2$·[16]aneS_4 (**2**) are high-spin iron(II) compounds that may be described as either octahedral or square-planar coordinated complexes. Mössbauer measurements on **1** at various temperatures and applied fields analyzed with the spin-Hamiltonian formalism together with spin-polarized molecular orbital calculations in local density approximation clearly favor the octahedral description. Calculations with different iron−iodine bond lengths elucidate the structural dependence of Mössbauer parameters and orbital energies during the gradual transition from octahedral to square-planar like coordination. A suggestion for the geometry of **2** ($d_{Fe,Br}$ = 2.47 Å) is obtained by minimizing the total binding energy. MO calculations provide evidence that unusually large iron−sulfur bond distances in **1** and **2** are forced by the size of the macrocycle [16]aneS_4 and are connected with unusually large axial bond distances.

1. Introduction

The possibility that iron in addition to molybdenum takes part in the biological nitrogen fixation processes[1] has prompted an investigation of the chemistry of iron in sulfur-containing environments.[2] We initially investigated iron and some tetrathioethers because they seemed particularly attractive for preliminary preparative studies, although it is unlikely that thioethers play a significant part in nitrogenase function.[3] No evidence of nitrogen fixation activity on reducing iron(II) adducts of cyclic thioethers was obtained, and almost always the sulfur ligands were lost from iron coordination. Our iron−thioether compounds seem, however, model compounds to study the influence of changes of structural properties upon redox potentials, because it is not at all obvious why the ferredoxins, which overwhelmingly have the same cysteinyl residues as ligands, have potentials in the range −250 to −650 mV.[4] The reason must lie in small structural differences.

The Mössbauer parameters of the 1:1 adducts of FeX_2 (X = Br or I) with 1,5,9,13-tetrathiacyclohexadecane seemed characteristic of five-coordinate iron(II) species, and appropriate crystal-structure determinations[2] showed that for X = I the Fe−I bond length is *ca.* 2.9 Å (Table 1), which is much larger than the usual Fe−I bond lengths and close to the sum of the corresponding ionic radii.

For these reasons it was not clear as to whether the compounds are best described as square-planar or as octahedral high-spin iron(II). A direct way to differentiate between the two possibilities consists in determining the sign of the electric field gradient, V_{zz}, which should be positive if the orbital d_{xy} were doubly occupied and lowest in energy (octahedral) and negative if d_{z^2} were lowest in energy (square-planar). In order to make this distinction, Mössbauer measurements on [Fe([16]-aneS_4)I_2] (**1**, Figure 1) and [Fe([16]aneS_4)Br_2] (**2**) in applied magnetic fields have now been carried out and completed with spin-polarized molecular orbital calculations in local density approximation.

Table 1

complex	d(Fe,L) (Å)	d(Fe,I) (Å)	*S*	coordination no.	ref
$[FeI_2(depe)_2]$[a]	2.31 (P)	2.71	0	6	21
[FeI(opdp)$_2$][b]	2.34 (P)	2.64	2	5	21
[Fe([16]ane S_4)]I_2	2.48 (S)	2.89	2	6	2
$[LH_3FeI]I$[c]	2.05 (N)	2.62	2	5	22

[a] depe = $Et_2PCH_2CH_2PEt_2$. [b] opdp = *o*-phenylenebis(diphenylphosphine). [c] L^{3-} = pentane-2,4-dione bis(*S*-alkylisothiosemicarbazonate).

2. Experimental Results

2.1. Mössbauer Measurements. Mössbauer measurements have been performed on a polycrystalline sample of compound **1** at various temperatures (4.2−180 K) and applied fields (0.02−6.26 T). The recorded spectra together with corresponding fits or simulations are shown in Figures 2 and 3. A least-squares fit of the spectrum in Figure 2 with Lorentzian lines yields the following: isomer shift $\delta_{\alpha-Fe}$ = 0.955 (4) mm s^{-1}, quadrupole splitting ΔE_Q = 4.073 (9) mm s^{-1}, and linewidth Γ = 0.334 (9) mm s^{-1}. The values are in agreement with those published earlier.[5] The value of the isomer shift is a clear indication for a ferrous high-spin complex. The quadrupole splitting is unusually large and temperature-independent.

2.2. Spin-Hamiltonian Analysis. Those spectra which have been recorded in a large applied field were analyzed by the spin-Hamiltonian formalism.[6] This approximation is justified here due to the rather large separation of the orbital ground state from the excited states, as indicated by the temperature-independent quadrupole splitting. Such an analysis aims at finding a unique set of parameters (zero-field splitting *D*, rhombicity *E*/*D*, sign V_{zz}, asymmetry η, hyperfine coupling A_i, $i = x, y, z$) which allows us to consistently simulate all measured spectra.

Zero-field parameters *D* and *E* of paramagnetic iron (here with spin *S* = 2) can be derived from field- and temperature-dependent Mössbauer spectra. The eigenstates of the spin quintet and the corresponding spin

[†] Medizinische Universität zu Lübeck.
[‡] University of Sussex.
[§] University of Essex.
[⊗] Abstract published in *Advance ACS Abstracts,* November 1, 1995.

(1) Eady, R. R.; Leigh, G. J. *J. Chem. Soc., Dalton Trans.* **1994**, 2739−2741.
(2) Hughes, D. L.; Jimenez-Tenorio, M.; Leigh, G. J.; Houlton, A.; Silver, J. *J. Chem. Soc., Dalton Trans.* **1992**, 2033−2037.
(3) Leigh, G. J. *Eur. J. Biochem.* **1995**, *229*, 14−20.
(4) Silver, J., Ed. In *Chemistry of Iron*; Blackie Academic & Professional: Glasgow, 1993; pp 201−202.
(5) Hills, A.; Hughes, D. L.; Jimenez-Tenorio, M.; Leigh, G. J.; Houlton, A.; Silver, J. *J. Chem. Soc., Chem. Commun.* **1989**, 1774−1775.
(6) Trautwein, A. X.; Bill, E.; Bominaar, E. L.; Winkler, H. *Struct. Bonding* **1991**, *78*, 1−95.

0020-1669/95/1334-6244$09.00/0

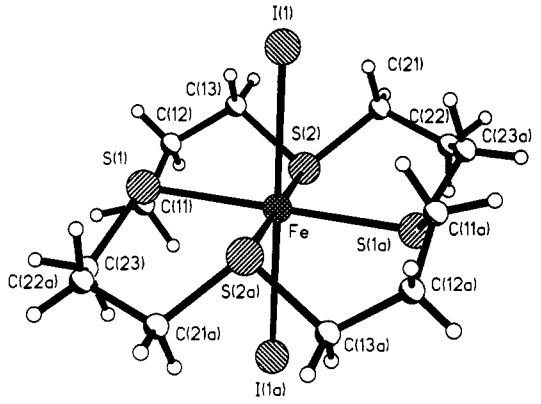

Figure 1. The molecular structure of [Fe([16]aneS_4)I_2]. The atom numbering illustrates the C_{2h} symmetry of the complex.

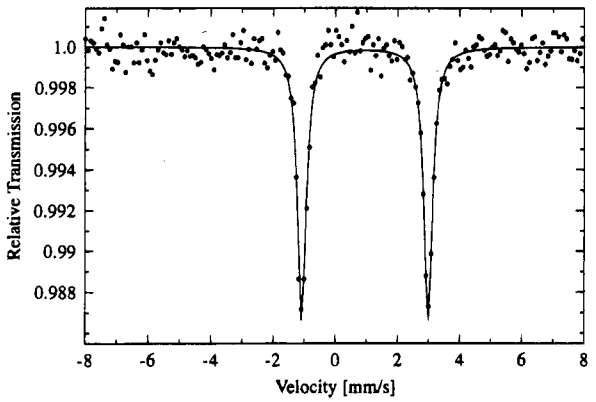

Figure 2. Experimental Mössbauer spectrum of complex **1** at 4.2 K and in an applied field of 20 mT. Solid line: Least-squares fit using Lorentzian lines yields $\delta_{\alpha\text{-Fe}} = 0.955$ (4) mm s^{-1}, $\Delta E_Q = 4.073$ (9) mm s^{-1}, and $\Gamma = 0.334$ (9) mm s^{-1}.

expectation values depend on the applied field, on temperature, and on D and E. This dependence is reflected in the measured internal field and therefore allows the determination of D and E either by varying the applied field at a fixed temperature or by varying the temperature at a fixed applied field.

It proved impossible at first to derive a unique parameter set reproducing the correct field and temperature dependence of the measured spectra. For a moderate applied field ($B_{app} \sim 2$ T), the calculated spin-expectation values appeared to be slightly too large using the parameter set which results from simulating the temperature dependence of high-field spectra ($B_{app} \sim 6$ T).

Therefore, in a second step, a demagnetization field ($\mathbf{B}_{dem}$) was included in the spin-Hamiltonian formalism in addition to the applied field. This field, which is sensed in addition to $\mathbf{B}_{app}$ by an iron ion in a solid, is assumed to be proportional to the spin-expectation values of the neighboring iron ions[7] and, hence, is induced in this model by the applied field. Consideration of the appropriate geometric arrangement of the next-nearest neighbors Fe_i yields

$$\mathbf{B}_{dem} = h_{dem} \sum_i \langle \mathbf{S}_i \rangle \qquad (1)$$

taking as parameter h_{dem} the same value for all next-nearest neighbors. Since the sample under study is polycrystalline, a powder summation was performed to account for the relative orientations of $\mathbf{B}_{dem}$ with respect to $\mathbf{B}_{app}$. With this approach a unique and consistent set of parameters has been found, allowing us to simulate all measured spectra (Figure 3).

In order to minimize the number of free parameters, the simulations were performed with $E/D = 0$, consistent with the approximately axial symmetry of the complex. This is not a severe constraint, as the simulated Mössbauer spectra are not very sensitive to variations of E/D. For the same reason, the g tensor could be varied between the free electron values $g = (2, 2, 2)$ and $g = (2.12, 2.12, 2.06)$, as derived from MO calculations (see below). Judged by the values $E/D = 0$ and $D > 0$, the ground state of the spin quintet is $|S = 2, S_z = 0\rangle$. This ground state exhibits spin-expectation values predominantly in the xy plane, so that the simulations are distinctly less sensitive to variations of A_z (the z-component of the hyperfine coupling tensor) than to variations of A_x and A_y. A summary of spin-Hamiltonian and Mössbauer parameters is given in Table 2. These parameters will be rationalized in the following section on the basis of ligand-field and molecular-orbital calculations.

3. Molecular Orbital Calculations

Electronic structure calculations within the one-electron approximation have been performed on **1** and **2**, containing 43 atoms and 118 valence electrons (61 spin-up and 57 spin-down electrons) each. For systems of this size, local density functional methods are more suitable than Hartree–Fock methods as they are considerably faster and—in the case of transition metal compounds—yield more reliable results. In this study, MO calculations have been carried out by the spin-polarized self-consistent-charge Xα method[8–10] with a basis set of 2s and 2p, 3s and 3p, 4s and 4p, and 5s and 5p orbitals for C, S, Br, and I, respectively, and of 3d, 4s, and 4p orbitals for Fe. The X-ray crystal structure of [Fe([16]aneS_4)I_2] has been used for the calculation on **1**, but no structural information is available for complex **2**. Under the simplifying assumption that all bond distances and angles within Fe([16]aneS_4) are equal in **1** and **2**, the iron–bromine bond length $d_{Fe,Br}$ has been determined to be 2.47 Å by minimizing the binding energy of compound **2** (Figure 6). This is somewhat larger than iron–bromine bond lengths reported for comparable iron–bromine compounds (2.403 Å, 2.413 Å).[11,12] The molecular orbital calculation for complex **2** is therefore based on the crystal structure of **1** and $d_{Fe,Br} = 2.47$ Å even though the charge density distribution obtained from the molecular orbital calculation described in detail in the next section indicates elongated iron–sulfur bonds.

3.1. Orbital Energies. The one-electron energy spectrum of **1** exhibits the typical pattern of high-spin iron(II) in a weakly distorted octahedral environment (Figure 4a). The exchange splitting between the stabilized Fe(3d) spin-up orbitals and the destabilized spin-down orbitals amounts to about 3.5 eV. The HOMO and the four lowest unoccupied MOs are spin-down orbitals with predominant Fe(3d) character and form two groups of MOs, which arise from the t_{2g} and e_g terms of ideal octahedral symmetry and are separated by about 0.9 eV. Therefore, as the octahedral splitting is considerably smaller than the exchange splitting, the ground state of the complex corresponds to a ferrous high-spin configuration ($S = 2$). Due to the axial distortion of the octahedral iron environment, the t_{2g} is split into d_{xy} and the nearly degenerate d_{xz} and d_{yz}, while the e_g is split into d_{z^2} and $d_{x^2-y^2}$. The HOMO has almost pure iron character (99% d_{xy}) since the long iron–sulfur bond distance (2.48 Å) does not allow for appreciable in-plane π interactions between Fe and S. This distance is about 0.7 Å larger than the sum of the corresponding atomic radii, whereas the iron–iodine

(7) Zimmermann, R.; Trautwein, A. X.; Harris, F. E. *Phys. Rev.* **1975**, *B12*, 3902–3907.
(8) Grodzicki, M. *J. Phys.* **1980**, *B13*, 2683–2691.
(9) Grodzicki, M. *Theorie und Anwendungen der Self-Consistent-Charge-Xα Methode*, Thesis of Habilitation, Hamburg, 1985.
(10) Bläs, R.; Guillin, J.; Bominaar, E. L.; Grodzicki, M.; Marathe, V. R.; Trautwein, A. X. *J. Phys.* **1987**, *B20*, 5627–5637.
(11) Sacconi, L.; Di Vaira, M. *Inorg. Chem.* **1978**, *17*, 810–815.
(12) Whitener, M. A.; Bashkin, J. K.; Hagen, K. S.; Girerd, J.-J.; Gamp, E.; Edelstein, N.; Holm, R. H. *J. Am. Chem. Soc.* **1986**, *108*, 5607–5620.

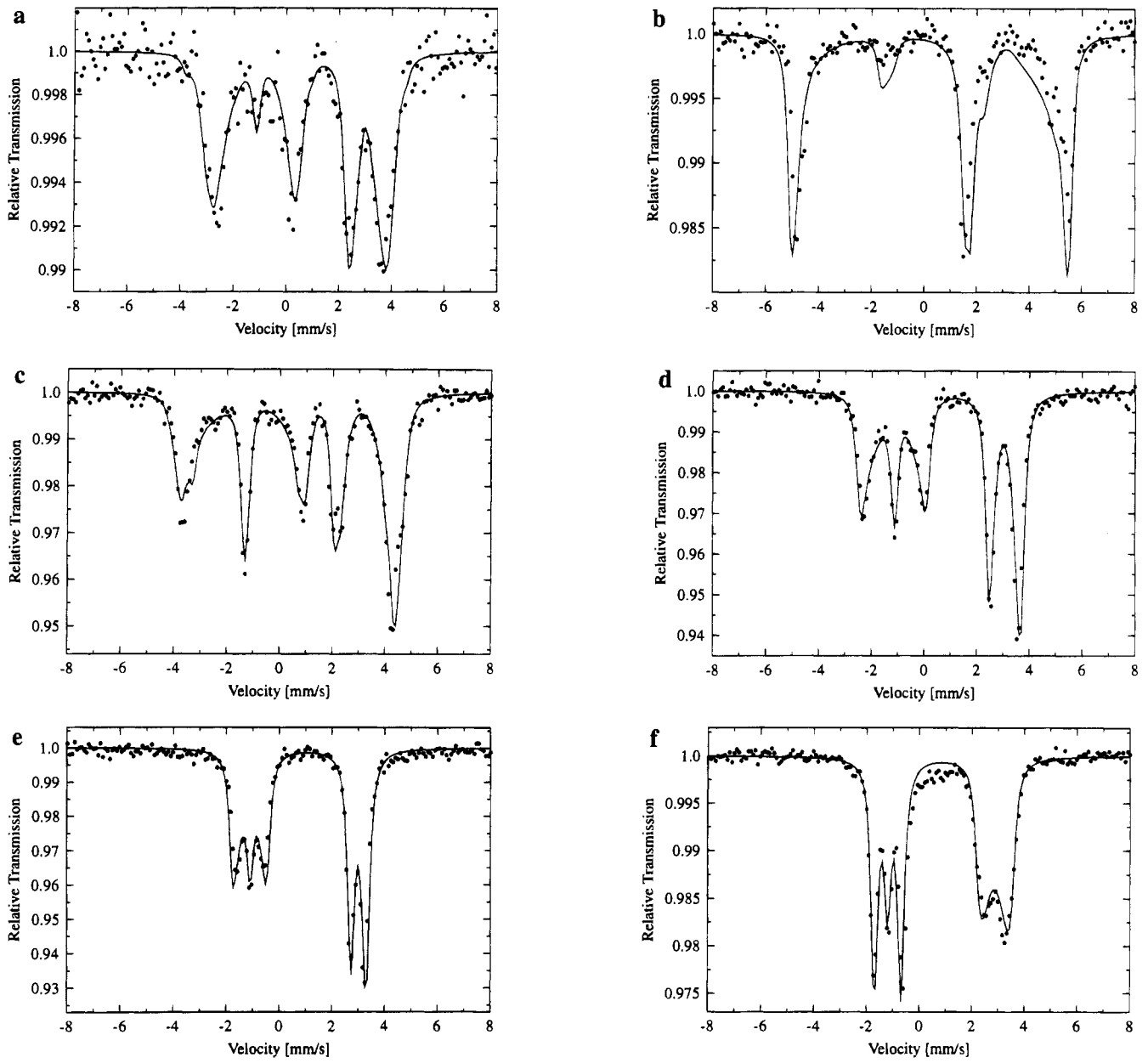

Figure 3. Experimental Mössbauer spectra of complex **1** at 4.2 K in applied fields of 2.02 $T \parallel \gamma$ (a) and 6.26 $T \parallel \gamma$ (b), and in an applied field of 6.26 $T \perp \gamma$ at 10 K (c), 20 K (d), 30 K (e), and 180 K (f). Solid lines: Simulations using the set of parameters given in Table 2.

Table 2. Spin-Hamiltonian Parameters Derived from Simulating Mössbauer Spectra for [Fe([16]aneS$_4$)I$_2$]

$\delta_{\alpha-Fe}$ (mm s^{-1})	Γ (mm s^{-1})	ΔE_Q (mm s^{-1})	sign V_{zz}	η	D (cm^{-1})	E/D	$g_{x,y,z}$	$A_{x,y}$ (T)	A_z (T)	h_{dem} (T)
0.95[a]	0.33[a]	4.07[a]	+	0	6.0	0	2[b]	−19.5	−19.5[c]	1.3[d]

[a] Taken from Figure 2. [b] Not sensitive to simulation if values $g_{x,y} = 2.12$ and $g_z = 2.06$, as derived from MO calculations, are used. [c] Not sensitive to simulation if value is changed by ±50%. [d] Parameter for demagnetization field $\mathbf{B}_{dem} = h_{dem}\sum_i \langle \mathbf{S}_i \rangle$.

bond distance (2.89 Å) is close to the sum of the atomic radii. Accordingly, a weak π interaction between iron and iodine with an admixture of about 2% I(5p) to d_{xz} and d_{yz} is observed. For both spin-up and spin-down electrons, the d_{xy} is lower in energy than d_{xz} and d_{yz}, indicating that the splitting between d_{xy} and the almost degenerate d_{xz} and d_{yz} is dominated by electrostatic repulsion rather than by covalent interaction. However, the order of t_{2g} and e_g is reversed for spin-up electrons, indicating that covalent interaction is responsible for the splitting between t_{2g} and e_g. The σ interactions between Fe on the one hand and S and I on the other lead to an admixture of S(3p) and I(5p) orbitals with the antibonding metal orbitals $d_{x^2-y^2}$ and d_{z^2}, respectively.

The analysis of the one-electron spectrum clearly favors a description of **1** as a slightly distorted octahedral complex rather than a square-planar one. The reason is easily understood with the results of model calculations for different Fe−I bond distances. The resulting orbital pattern of the five spin-down MO's with predominant Fe(3d) character is displayed in Figure 5. In order to facilitate comparison, the energy of the d_{xy} orbital has been chosen as zero of energy in each case. As expected, the covalency of the d_{z^2}-like molecular orbital and its energy decrease strongly with increasing Fe−I separation, whereas the remaining four orbitals undergo only minor changes. For an Fe−I distance of 3.5 Å, the splittings between d_{xy}, $d_{xz,yz}$, and d_{z^2} orbitals become equally small (Figure 5), and the 3d

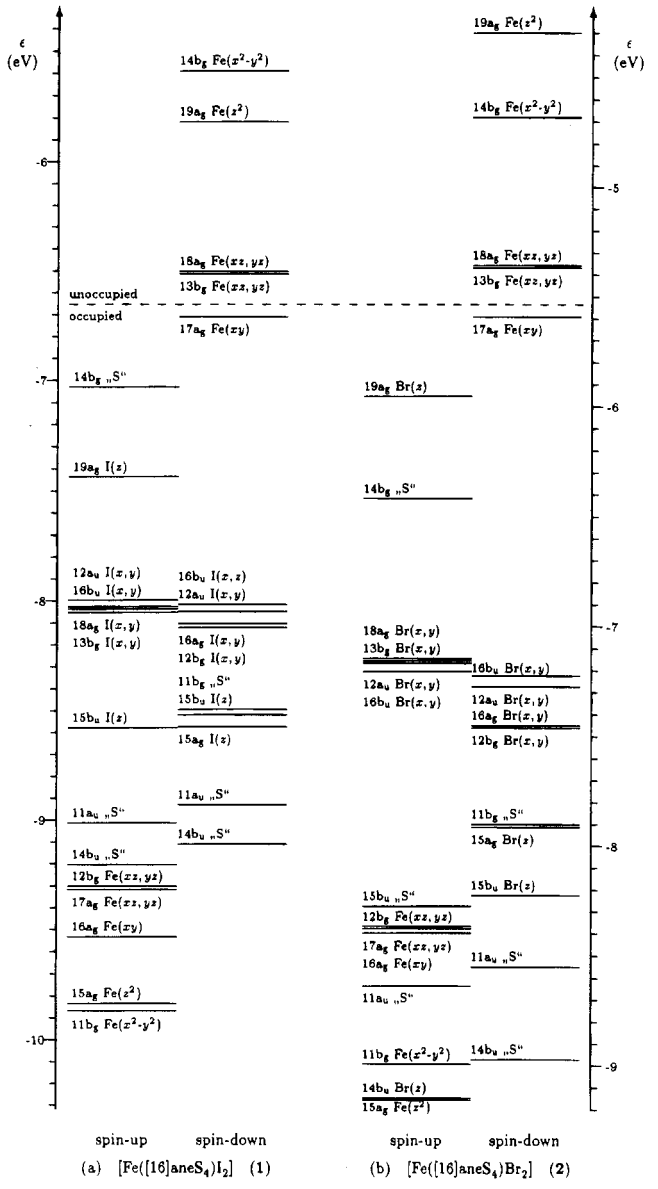

Figure 4. One-electron spectra of **1** and **2**, calculated with a spin-polarized SCC Xα MO method. MOs are labeled according to the irreducible representations of the molecular point group C_{2h}.

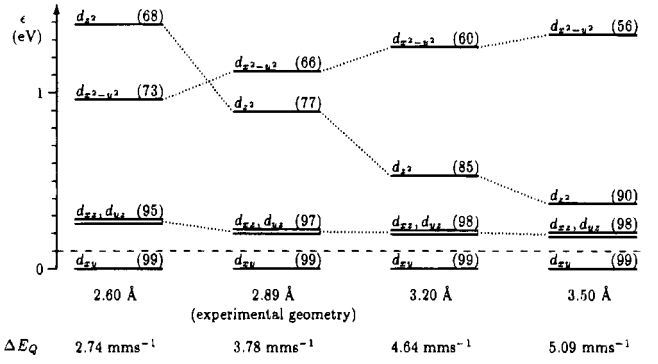

Figure 5. MO energies of the five spin-down MOs with predominant Fe(3d) character, depending on Fe−I bond distance, together with corresponding calculated quadrupole splittings ΔE_Q. The value 2.89 Å corresponds to the experimental Fe−I bond distance.

characters of these orbitals are similar. Since the sulfur atoms are almost neutral for any Fe−I separation, the d_{xy} orbital is always below the d_{z^2} orbital. It follows that complex **1** cannot be described as square-planar at the experimental geometry.

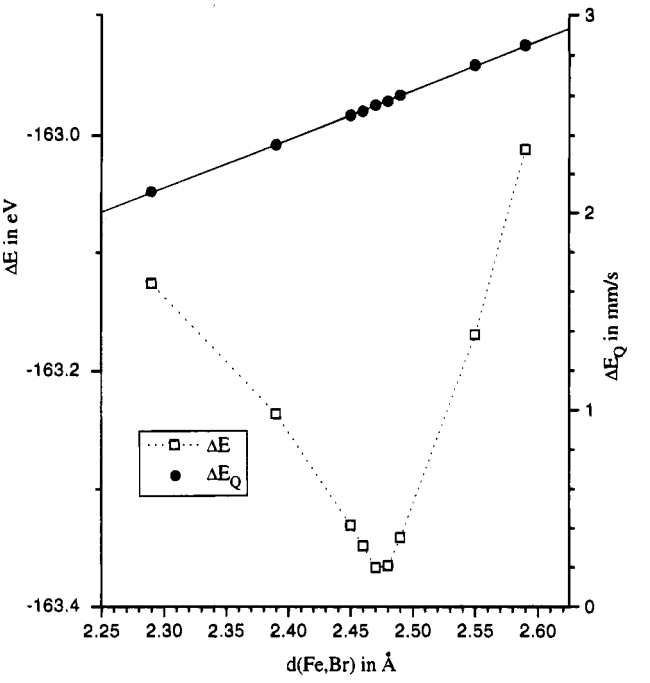

Figure 6. Calculated binding energies ΔE and quadrupole splittings ΔE_Q of complex **2** in the dependence of the iron−bromine bond length $d_{Fe,Br}$.

The orbital energies of **2** (Figure 4b) resemble closely those of **1**. The main difference in bonding is the stronger covalent interaction between the iron and the halogen atoms in **2**, which reduces the positive effective charge of the iron atom. The reduced charge yields a uniform destabilization of the Fe(3d) orbitals whereas the stronger covalent interaction concerns the antibonding d_{z^2} orbital in particular. The overall destabilization increases the energy gap between Fe(3d) and S(3p) orbitals and leads to a weaker covalent interaction between Fe and S, as indicated by the reduced overlap populations of the respective bonds. Such a reduced covalent interaction usually leads to increased bond distances. In order to investigate the influence of the iron−sulfur bond length ($d_{Fe,S}$) on $d_{Fe,Br}$, a molecular geometry with four SH_2 groups instead of [16]aneS_4 has been used as a simplified model of compound **2**. The binding energy of this model as a function of $d_{Fe,Br}$ is shown in Figure 7 for different iron−sulfur bond lengths. These calculations demonstrate that the binding energy is lowered if $d_{Fe,S}$ decreases and thereby confirm that the unusually long iron−sulfur bond distances are forced by the size of [16]aneS_4. Furthermore, the evidence is that an increased iron−sulfur bond length favors larger iron−halogen bond lengths, which may also be interpreted in the way that the axial acceptor power of Fe increases with decreasing Fe−S distance. The dependence of $d_{Fe,Br}$ on $d_{Fe,S}$ can be described quantitatively by the ratio $\delta d_{Fe,Br}/\delta d_{Fe,S} \approx 1.5$ for distances close to the iron−sulfur bond length in compound **1**. Hence, an iron−bromine bond length of 2.47 Å has to be considered as a lower limit.

3.2. Quadrupole Splitting. The measured quadrupole splitting ΔE_Q is related to the electric field gradient (efg) V_{zz} at the Mössbauer nucleus by

$$\Delta E_Q = {}^1/_2 eQV_{zz}\sqrt{1+\eta^2/3} \qquad (2)$$

where $Q = 0.15$ barn is the nuclear quadrupole moment of the first excited state of ^{57}Fe.[13,14] Due to the almost perfect axial

(13) Lauer, S.; Marathe, V. R.; Trautwein, A. X. *Phys. Rev.* **1979**, *A19*, 1852−1861.

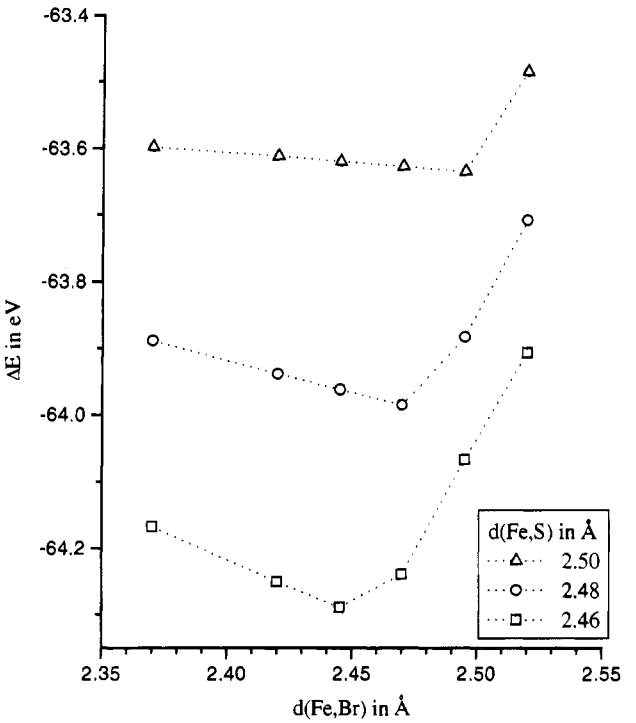

Figure 7. Calculated binding energies ΔE of a simplified model of complex **2** in the dependence of the iron−bromine bond length $d_{Fe,Br}$.

symmetry, the asymmetry parameter is close to zero for both complexes. Core polarization effects are taken into account by the Sternheimer shielding function $\gamma(r)$ derived from atomic self-consistent first order perturbation calculations;[13] an analytical representation of $\gamma(r)$ is given in ref 15. Apart from these approximations, the efg is computed rigorously within the frame of a valence-electron-only MO method.[16] The calculated efg for **1** and **2** is split into a valence and a ligand contribution (Table 3). Apparently, the valence contribution to the efg is dominating; the ligand contribution is smaller by one order of magnitude. The calculated quadrupole splitting for complex **1** is about 7% smaller than the experimental value, whereas the discrepancy between calculated and observed quadrupole splitting is about 29% for complex **2**, probably due to an improper choice of the geometry. For instance, if the iron−sulfur bond length were 2.53 Å instead of 2.48 Å, an iron−bromine distance of about 2.55 Å would be expected (Figure 7). This increase in $d_{Fe,S}$ as well as in $d_{Fe,Br}$ enhances ΔE_Q by about 0.22 mm s^{-1}.

Since the valence contribution is dominant in **1** and **2**, the calculated efg is roughly equal to the expression

$$\Delta n_{3d}\langle r^{-3}\rangle(1 - R)(4/7) \tag{3}$$

where

$$\Delta n_{3d} = n_{xy} + n_{x^2-y^2} - n_{z^2} - (n_{xz} + n_{yz})/2 \tag{4}$$

defines the anisotropy of the Fe(3d) shell (Table 4). In the ligand-field picture, the d_{xy} orbital should be doubly occupied, and the remaining four Fe(3d) orbitals should be singly occupied, resulting in an anisotropy of unity and a quadrupole splitting of about 4 mm s^{-1}. However, covalent interactions

(14) Bominaar, E. L.; Guillin, J.; Sawaryn, A.; Trautwein, A. X. *Phys. Rev.* **1989**, *B39*, 72−79.
(15) Grodzicki, M.; Lauer, S.; Trautwein, A. X.; Vera, A. *Adv. Chem. Ser.* **1981**, *194*, 3−37.
(16) Grodzicki, M.; Männing, V.; Trautwein, A. X.; Friedt, J. M. *J. Phys.* **1987**, *B20*, 5595−5625.

Table 3. Quadrupole Splitting

	ΔE_Q (mm s^{-1})				η	
complex	exptl	calcd	valence	ligand	exptl	calcd
[Fe([16]aneS$_4$)I$_2$]	+4.07[a]	+3.78	+4.11	−0.41	0	0.01
[Fe([16]aneS$_4$)Br$_2$]	3.60[b]	+2.55	+3.06	−0.32		0.02

[a] At 4.2 K. [b] At 77 K.

Table 4. Anisotropy of Fe(3d) Orbital Occupation

	n_{3d}					
complex	xy	xz	yz	z^2	x^2-y^2	Δn_{3d}
[Fe([16]aneS$_4$)I$_2$]	1.99	1.02	1.02	1.20	1.28	1.05
[Fe([16]aneS$_4$)Br$_2$]	1.99	1.05	1.05	1.26	1.20	0.88

lead to noninteger occupation numbers: the $d_{x^2-y^2}$ and d_{z^2} orbitals form σ bonds with S(3p) and I(5p) orbitals, respectively. Furthermore, d_{xz} and d_{yz} orbitals are admixed to I(5p) orbitals, forming π-bonding MOs. Hence, increasing covalent interactions between the iron atom and the halogen atoms will increase the occupation of d_{xz}, d_{yz}, and d_{z^2} orbitals, thereby decreasing the efg, and *vice versa*. For instance, an Fe−I separation of 3.20 Å in **1** leads to a calculated quadrupole splitting of 4.64 mm s^{-1} instead of 3.78 mm s^{-1} for an Fe−I separation of 2.89 Å. Therefore, we conclude that a slightly larger covalent interaction between iron and bromine in comparison to iron and iodine may account for the observed reduction of the quadrupole splitting in complex **2**.

3.3. Zero-Field Splitting and Related Parameters. Taking Δ_1 and Δ_2 as the orbital energy difference between the HOMO (d_{xy}) and the $d_{xz,yz}$ and the $d_{x^2-y^2}$ orbital, respectively:

$$\Delta_1 = \epsilon_{xz,yz} - \epsilon_{xy} \approx 1656\ \text{cm}^{-1}$$

$$\Delta_2 = \epsilon_{x^2-y^2} - \epsilon_{xy} \approx 9025\ \text{cm}^{-1}$$

various hyperfine parameters can be derived from the following estimates:[6]

- zero-field splitting

$$D = \lambda^2\left(\frac{\kappa_1}{\Delta_1} - \frac{4\kappa_2}{\Delta_2}\right) \approx 3\ \text{cm}^{-1} \tag{5}$$

- effective g values

$$g_{x,y} = 2 - 2\kappa_1\lambda/\Delta_1 \approx 2.12 \tag{6}$$

$$g_z = 2 - 8\kappa_2\lambda/\Delta_2 \approx 2.06$$

- effective magnetic moment at room temperature

$$\mu_{\text{eff}} = \sqrt{(g_x^2 + g_y^2 + g_z^2)/3S(S+1)}\mu_B \approx 5.15\mu_B \tag{7}$$

where a value $\lambda = 101\ \text{cm}^{-1}$ for the spin-orbit coupling constant as well as the constants $\kappa_1 = 0.96$ and $\kappa_2 = 0.65$ describing covalency effects as derived from the MO calculations have been used. If the perturbation approximation leading to eq 5 is expanded to higher orders in λ, a slightly enhanced value of $D = 3.5\ \text{cm}^{-1}$ is obtained for the zero-field splitting. However, since the accuracy of orbital energy differences derived from MO calculations for such a big system is certainly not better than 0.1 eV, the calculated values for D and $g_{x,y,z}$ have to be taken with caution. An alternative estimate of the zero-field splitting D is provided by making use of the fact that ΔE_Q is practically temperature-independent in the range between 4.2 and 180 K. Taking

$$\Delta E_Q(T) = \Delta E_Q(0)\frac{1 - \exp(-\Delta_1/kT)}{1 + 2\exp(-\Delta_1/kT)} \quad (8)$$

a lower limit of 700 cm^{-1} for Δ_1 is estimated. Substituting this value into eq 5 yields an upper limit of 9 cm^{-1} for D.

The hyperfine coupling tensor A is related to the internal field $\mathbf{B}_{int}$, which can be expressed as sum of the isotropic Fermi contact term and the anisotropic orbital and spin-dipolar terms.[17] From the MO calculation, an isotropic contribution of −21.1 T (−23.9 T) is derived. Together with the anisotropic contributions of +2.1 T to $A_{x,y}$ and +9.2 T to A_z, the final values for the **A** tensor are

$$A_{x,y} = -19.0\ \text{T}\ (-21.8\ \text{T}) \quad (9)$$

$$A_z = -11.9\ \text{T}\ (-14.7\ \text{T})$$

The values in parentheses are obtained if the Fermi contact term is derived using the total spin $S = 2$ instead of that part being localized in the Fe(3d) shell (S_{3d}).[18] The range of parameters 3 $cm^{-1} < D < 9\ cm^{-1}$, $-19.0\ \text{T} < A_{x,y} < -21.8$ T, and $-11.9\ \text{T} < A_z < -14.7$ T as derived from the MO calculation is thus consistent with the parameters derived from the spin-Hamiltonian analysis of magnetic Mössbauer spectra. Furthermore, the calculated magnetic moment at room temperature, $\mu_{eff} = 5.15\mu_B$, is close to the value obtained experimentally[2] ($5.13\mu_B$).

4. Conclusion

It has been shown that complex **1** is best described as having a distorted octahedral environment despite the large Fe−I distance. Both the observed and calculated quadrupole splittings are positive, and the theoretical value is just 7% smaller than the experimental value. For compound **2** the measured quadrupole splitting is about 10% smaller, which may be rationalized by a slightly larger iron−bromine covalent interaction than the iron−iodine interaction. The calculated efg is about 29% smaller than the observed value, which may be due to an improper choice of geometry. However, this geometry was based on that of compound **1**, except for the shorter iron−halogen bond distances. A slight increase of this distance might account partly for the discrepancy between observed and calculated values.

The parameters D, $A_{x,y}$, and A_z derived from the MO calculations for compound **1** are qualitatively consistent with the parameters derived from the spin-Hamiltonian analysis of the Mössbauer spectra, and the calculated magnetic moment at room temperature is close to the experimental value. The MO calculations demonstrate that the Mössbauer parameters are very sensitive to the iron−halogen bond lengths, at least when [16]-aneS_4 is the coligand, and give confidence that the description of the bonding in compounds **1** and **2** is basically correct.

The correlations between axial and equatorial bond distances and the corresponding bond strengths are surprising at first sight. In compound **1** the iron−sulfur separations are very long, and the easy loss of the thioether under mild conditions suggests that the iron−sulfur interactions are not very strong. It is not obvious what radii one should choose to evaluate the bond lengths, but if one takes normal covalent radii for iron and sulfur, then the iron−sulfur bonds are *ca.* 0.2 Å too long. That would intuitively lead one to expect that the iron−iodine bonds should be short, but the converse is observed, to the extent of about 0.4 Å. This is confirmed by the fact that compound **1** is synthesized by direct reaction of the iodide and the thioether in acetonitrile, from which it crystallizes without any coordinated acetonitrile. The acceptor power in the axial direction must be very weak. On the other hand, if one attempts the same reaction, but with [14]aneS_4 in place of [16]aneS_4, then the complex product is cationic, $[Fe(MeCN)_2([14]aneS_4)]^{2+}$. The smaller cycle clearly allows the closer approach of the sulfur atoms to the iron, and this also increases the axial acceptor power. This finds support in the molecular orbital calculations yielding smaller Fe−Br distances with decreasing Fe−S distances. This discussion emphasizes the dangers in assuming that the radius of an atom or ion is determined only by its oxidation state or its ionicity and shows clearly that such a radius depends also on the bond direction in which it is estimated. It also shows that it is unwise to infer bonding quality (strength and type) from simple bond length considerations as has been shown earlier.[19,20]

The proper choice of equatorial ligands should enable one to control spin state and lability of axial ligands. This is apparently so in porphyrin−iron(II) chemistry as well as in phosphine−iron(II) chemistry. Similar effects have already been extensively explored in cyclazane−nickel(II) chemistry. The results presented here might help to determine the factors which control similar sulfur−iron(II) chemistry.

Acknowledgment. Support from the EU Human Capital and Mobility grant to the MASIMO network (ERBCHRX-CT-9200 72) and from the Deutsche Forschungsgemeinschaft is gratefully acknowledged.

IC950528I

(17) Marathe, V. R.; Trautwein, A. X. In *Advances in Mössbauer Spectroscopy*; Thosar, B. V., Iyengar, P. K., Eds.; Elsevier: Amsterdam, 1983, Chapter 7.

(18) Paulsen, H.; Ding, X.-Q.; Grodzicki, M.; Butzlaff, Ch.; Trautwein, A. X.; Hartung, R.; Wieghardt, K. *Chem. Phys.* **1994**, *184*, 149−162.

(19) Elbel, S.; Blanck, A.; Walther, H.; Grodzicki, M. *J. Chem. Soc., Faraday Trans. 2* **1985**, 869−880; *J. Chem. Soc., Faraday Trans. 2* **1986**, 971.

(20) Grodzicki, M.; Elbel, S. In *Modelling of Structure and Properties of Molecules*; Maksic, Z. B., Ed.; Ellis Horwood: Chichester, 1987; pp 239−250.

(21) Barclay, J. E.; Hills, A.; Hughes, D. L.; Leigh, G. J. *J. Chem. Soc., Dalton Trans.* **1988**, 2871−2877.

(22) Knof, U. PhD Thesis, Bochum, 1995. Publication in preparation.